Eur. Phys. J. B **65**, 57–64 (2008)
DOI: 10.1140/epjb/e2008-00322-7

THE EUROPEAN PHYSICAL JOURNAL B

In situ SAXS study on size changes of platinum nanoparticles with temperature

W. Wang[1], X. Chen[1], Q. Cai[1], G. Mo[1], L.S. Jiang[1], K. Zhang[1], Z.J. Chen[1], Z.H. Wu[1,a], and W. Pan[2]

[1] Beijing Synchrotron Radiation Facility, Institute of High Energy Physics, Chinese Academy of Sciences, & Graduate University of Chinese Academy of Sciences, Beijing 100049, P.R. China
[2] Jiangxi Institute of Measurement and Testing, Nanchang 330002, P.R. China

Received 20 September 2007 / Received in final form 8 April 2008
Published online 9 August 2008

Abstract. Poly(vinylpyrrolidone) (PVP)-coated platinum (Pt) nanoparticles were prepared in methanol-water reduction method. In situ small-angle X-ray scattering (SAXS) and X-ray diffraction (XRD) techniques were used to probe the size change of particles and crystallites with temperature. Tangent-by-tangent (TBT) method of SAXS data analysis was improved and used to get the particle size distribution (PSD) from SAXS intensity. Scherrer's equation was used to derive the crystallite size from XRD pattern. Combining SAXS and XRD results, a step-like characteristic of the Pt nanoparticle growth has been found. Three stages (diffusion, aggregation, and agglomeration) can be used to describe the growth of the Pt nanoparticles and nanocrystallites. Aggregation was found to be the main growth mode of the Pt nanoparticles during heating. The maximum growth rates of Pt nanoparticles and Pt nanocrystallites, as well as the maximum aggregation degree of Pt nanocrystallites were found, respectively, at 250 °C, 350 °C and 300 °C. These results are helpful to understanding the growth mode of nanoparticles, as well as controlling the nanoparticle size.

PACS. 61.46.Df Structure of nanocrystals and nanoparticles – 65.80.+n Thermal properties of small particles, nanocrystals, and nanotubes

1 Introduction

In recent decades, nanomaterials have attracted great interests and are widely studied because of their novel properties different from bulks. The nanoparticle size is one of the important factors to control the unique properties of nanomaterials. Usually, the smaller the nanoparticle size is, the more prominent the unique properties are. Therefore, people attempt to control the size of nanoparticles as small as possible in sample preparation. However, the nanoparticle size depends not only on the sample preparation, but also on the applied environment of nanomaterials including temperature and even radiation [1]. It is well known that the nanoparticle size will become larger with temperature increasing for most free nanomaterials. There have been some researches [2] on nanoparticles with in situ transmission electron microscopy (TEM) observation and in situ X-ray diffraction (XRD) measurement during heating. Several growth modes of nanoparticles, for example, Ostwald ripening [3], fusion [4], coalescence [5], condensation [6], coagulation [7] and so on, have been found by TEM direct observation. Obviously, the structural and thermal stability of nanomaterials are very important for their potential application. In order to utilize well the unique properties of nanomaterials, it is necessary to study the growth mode of nanoparticles.

Studying the size change of nanoparticle with temperature is helpful to understand the thermal stability of nanomaterials. In the past, TEM observation and XRD measurement are often used to research the structural changes of nanomaterials. With the development of X-ray technology, especially the application of synchrotron radiation source, small angle X-ray scattering (SAXS) technique is widely used as an effective measure to probe the nanoscale structures in materials [8]. In recent years, there is a burgeoning literature on the study of nanoparticle nucleation and growth probed by SAXS [9–11]. Usually, SAXS technique can give the information of the particle size, shape, size distribution and so on. In addition, SAXS technique can also get more statistically average result than TEM observation. In this paper, an in situ SAXS technique is used to study the structural change of Pt nanoparticles with temperature. First, the SAXS data analysis method for inorganic samples is briefly discussed, and then the size distribution of Pt nanoparticles is derived. The obtained result is helpful to understand the growth mechanism of nanoparticles.

[a] e-mail: wuzh@mail.ihep.ac.cn

2 Experiment

PVP-coated Pt nanoparticles were synthesized in methanol-water reduction method [12]. All the reagents were in analytical grade and were purchased from Beijing chemicals. All the water was deionized. The sample preparation is described as follows. First, 0.085 g PVP and 0.052 g $H_2PtCl_6{\cdot}6H_2O$ (CPA) were added to the mixture of 14 ml water and 126 ml methanol. After stirring for 0.5 h, the solution was refluxed for 3 h with an argon flow sweeping over the liquid layer. Next, the PVP-coated Pt colloid formed a transparent and homogeneous solution with dark-brown color. Finally, the PVP-coated Pt nanoparticles were precipitated by adding 500 ml acetone to the resulting solution. The precipitate was dried in air and was mixed with the powder of boron nitride (BN). This mixture was pressed into a pill as the as-prepared sample, and the adding BN was used as the support frame. Pure BN powder was also pressed into a pill and used to subtract the background from the support frame.

In situ SAXS experiments during heating the samples were carried out on the SAXS station at beamline 4B9A of Beijing Synchrotron Radiation Facility (BSRF). The storage ring was operated at 2.2 GeV with current about 80 mA. The incident x-ray wavelength was selected to be 0.154 nm by a double-crystal Si (111) monochromator. The SAXS data were collected with Mar345 on-line image-plate (IP) detector and the sample-to-detector distance was fixed at 1.5 m. SAXS data of the as-prepared sample and the BN background were, respectively, collected at 25 °C, 200 °C, 300 °C, 400 °C and 500 °C.

The XRD experiments were performed on the XRD station at beamline 4B9A of BSRF with the same measurement condition. In order to distinguish well the diffraction peaks of Pt nanoparticles from the background materials, LiF was chosen as the background materials to mix with Pt nanoparticles. The diffraction patterns were collected with a curved IP detector [13] with an angle accuracy of 0.01 °. The diffraction rings were obtained and were transformed into one-dimensional diffraction spectra, which were normalized by the incident X-ray intensity recorded with an ion chamber in front of the sample.

3 Data analysis

The original SAXS data were collected by Mar345 IP and saved as `*.mar3450` format. Firstly, these data files were transferred into two-dimensional digital data by using the software Fit2D [14]. The SAXS curves of intensity vs. scattering-vector were obtained by arc-integral or linear integral and the data analysis was performed by using SAXS1.0 [15].

Generally speaking, for a monodisperse system, for example, the biological macromolecule, the particle shape can be well derived by using international software [16]. For layer samples with thick substrate, IsGISAXS2.6 software [17] can be well used to simulate the structural information. However, for inorganic nanoparticles systems, their particle-sizes are usually multi-dispersive. In this case, the particle shape and particle size distribution (PSD) can not often be obtained at the same time. But there have been several methods [18–24] to derivate the PSD, for example, Shull-Roess method, Lognormal distribution fit, Regularization technique, Tangent-by-tangent (TBT) method, Polydispersity index (PDI) method, etc. Even so, only one or two methods can work well for a special inorganic system because of the complexity of the sample size and shape as well as the possible interference effect among particles and the lower signal-to-noise ratio (SNR) at larger scattering angle.

TBT method was described by Jellinek and Fankuchen early in 1946, it was used to estimate the discrete PSD of Al_2O_3 colloid with acceptable precision [20,25]. However, the X-ray scattering intensity often decays rapidly with the scattering angle increasing, and the SNR is not enough good at higher scattering angles. This limits the use of the TBT method. In order to validate this method in the whole data region, we introduce the cubic-spline-function to fit the scattering curve. Then the TBT method is improved to perform on the spline curve. For a polydisperse spherical system, the X-ray scattering intensity with Guinier approximation can be described as:

$$I(q) = I_e \int_0^\infty N(R_G)\rho^2 V^2(R_G) e^{-q^2 R_G^2/3} dR_G, \qquad (1)$$

where R_G is the radius of gyration, and N is the number of particles with R_G. V is the volume of particle with R_G. ρ is the electron density in particle with R_G. I_e is the scattering intensity of one electron. Assuming the system contains nanoparticles with several size levels, the above formula can be simplified to a sum function:

$$I(q) = I_e N_1 n_1^2 e^{-q^2 R_1^2/3} + I_e N_2 n_2^2 e^{-q^2 R_2^2/3} + \cdots + I_e N_i n_i^2 e^{-q^2 R_i^2/3}, \qquad (2)$$

where, i represents the ith size level. N_i and n_i are, respectively, the particle number and the electron number of the particle with gyration radius R_i. If we define

$$K_i = I_e N_i n_i^2. \qquad (3)$$

Then the X-ray scattering intensity at $q = 0$ is

$$I(0) = K_1 + K_2 + \cdots + K_i. \qquad (4)$$

Therefore, the volume percentage can be yielded by

$$W_1 : W_2 : \cdots : W_i = \frac{K_1}{R_1^3} : \frac{K_2}{R_2^3} : \cdots : \frac{K_i}{R_i^3}. \qquad (5)$$

The TBT method is illustrated in Figure 1. Firstly, the first tangent (curve b) is performed from the last data point of the logarithm plot (curve a), then the intercept (K_1) and the slope ($-R_1^2/3$) can be obtained. After subtracting curve $b(q^2)$ from curve $a(q^2)$ in linear intensity scale, intensity difference $c(q^2)$ can be obtained. Repeatedly the above procedure, the second tangent is performed

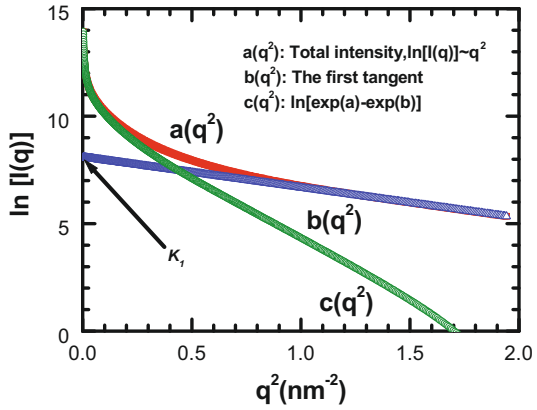

Fig. 1. Tangent-by-tangent method. Curve $a(q^2)$ is the scattering intensity plot in logarithmic scale, line $b(q^2)$ is the first tangent. From the slope and intercept of line $b(q^2)$, the first level particle's radius (R_1) and the volume content (K_1) can be obtained. Curve $c(q^2)$ is the intensity difference between $a(q^2)$ and $b(q^2)$ in linear intensity scale. The data point to perform other tangents is restricted by equation (6).

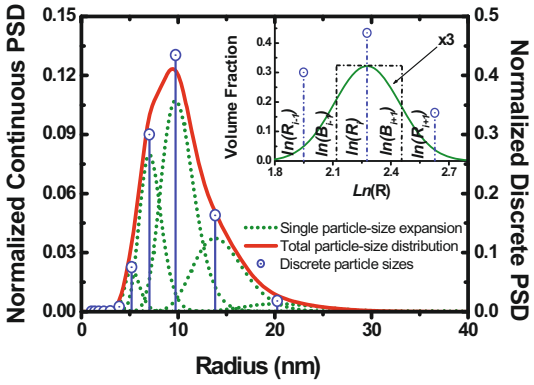

Fig. 2. Sketch map of distribution expansion for discrete particle sizes. Open circle (O) represents the known discrete particle sizes and occupancies; dot lines are the discrete particle-size expansion. Solid line is the normalized total particle size distribution. The expansion of one (9.7 nm) of the discrete particle sizes is described in the inset.

on curve $c(q^2)$. Finally, all the parameters (K_i, R_i) can be obtained. It is noticeable that the ith tangent is performed on the jth data point which should satisfy the following restrictive condition:

$$\begin{cases} \dfrac{d\left[\ln(c_j(q^2))\right]}{d(q^2)} \le \dfrac{d\left[\ln(c_{j+1}(q^2))\right]}{d(q^2)} \\ \dfrac{d^2\left[\ln(c_j(q^2))\right]}{\left[d(q^2)\right]^2} = 0. \end{cases} \tag{6}$$

By using TBT method, the corresponding particle sizes and contents can be estimated from the slopes and the intercepts of the tangents. Usually, several discrete particle sizes can be obtained, which depends on particle-size level inO the sample. Actually, each particle size is only an average result, which can be described as a narrow PSD function. In addition, an approximately continuous distribution is often expected for most application. Therefore, those discrete particle sizes obtained with TBT method can also be expanded with the lognormal distribution functions [26]. Figure 2 describes schematically the serialization of the discrete particle sizes. Here, a known discrete system is given with 11 different particle sizes and occupancies which could be the results of TBT. The ith discrete particle size can be substituted by the following formula:

$$P_i(R) = \frac{A_i}{\sqrt{2\pi}\sigma_i} \exp\left[-\frac{(\ln R - \ln R_i)^2}{2\sigma_i^2}\right], \tag{7}$$

where, R_i, σ_i and A_i are, respectively, the position, width and area of the ith PSD function. R_i can be taken as the value of the ith particle size, and A_i as the occupancy of the ith discrete particle. The HWHM ω_i (i.e., $\sqrt{\ln 4}\sigma_i$) of equation (7) is defined as:

$$\omega_i = \frac{\ln(R_{i+1}) - \ln(R_{i-1})}{4}. \tag{8}$$

For example, on the basis of equation (8), the FWHM of the distribution given by equation (7) is from $\ln(B_{i-1})$ to $\ln(B_{i+1})$ for the particle size of 9.7 nm as shown in the inset of Figure 2. Because equation (7) is a symmetrical function in $\ln(R)$ space, we have $\ln(B_{i+1}) - \ln(R_i) = \ln(R_i) - \ln(B_{i-1})$. For the minimum discrete particle size (for example, R_1), its lower R value (R_0) is taken as the value of $R_0 = \pi/q_{max}$. For the maximum discrete particle size (for example, R_N), its upper R value (R_{N+1}) is taken as the value of $R_{N+1} = \pi/q_{min}$. Where, q_{min} and q_{max} are the lower and upper limits of the scattering vector detected by the experiment. Finally, a quasi-continuous PSD function can be obtained by normalizing the summation of all the single distribution functions.

4 Results and discussion

The above SAXS data analysis method was firstly checked for a given discrete model system. This model system consists of seven discrete particle sizes and the corresponding occupancies as depicted in Figure 3a. The theoretical SAXS intensity for the given model system has been calculated as shown in Figure 3b. By using the above TBT method, seven discrete particle sizes can be well reproduced from the calculated SAXS intensity. Figure 3a compares the particle sizes and their occupancies between the given model system and the result reproduced by TBT method. It can be seen that the profile of the reproduced seven particle sizes is excellently agreement with the profile of the given seven particle sizes, i.e. the particle size distribution (PSD) can be excellently reproduced. But the reproduced particle sizes deviate gradually from the given ones with the particle-size increasing. This is because that the SAXS intensity decreases more fast for larger particles than smaller ones with scattering vector q increasing, therefore, the contribution of larger particle to high-q end of SAXS intensity is less than the contribution of smaller

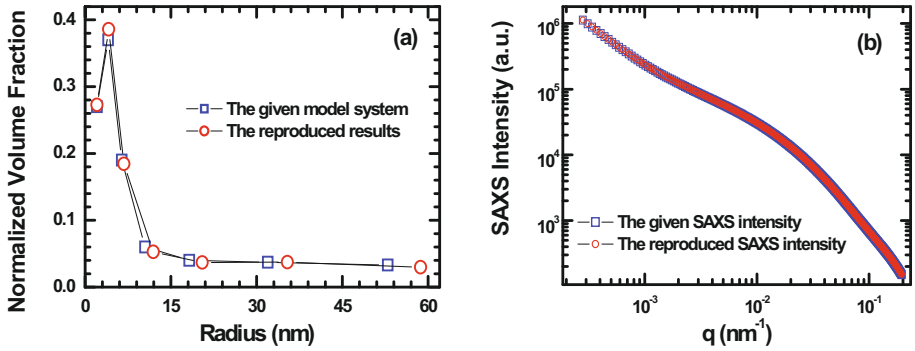

Fig. 3. Comparison of particle size distribution (a) and SAXS intensity (b) in logarithmic scale. In (a), the open squares represent the seven given discrete particles' sizes and the open circles are the results reproduced by TBT method. (b) Compares the corresponding SAXS intensities between the given model system and the reproduced one with TBT method.

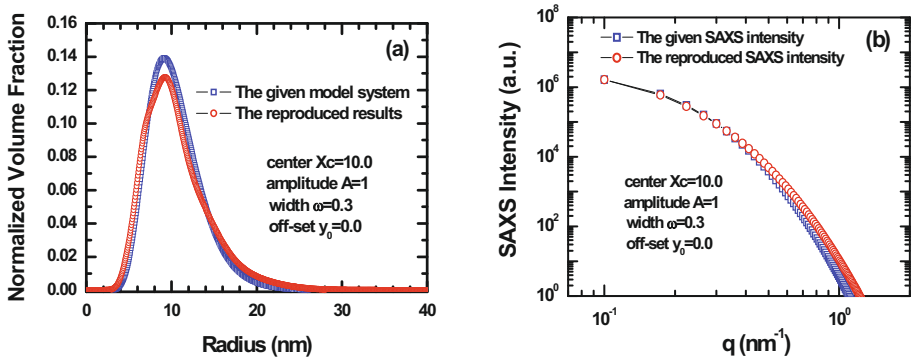

Fig. 4. Comparison of particle size distribution (a) and SAXS intensity (b) in logarithmic scale. In (a), the open squares represent the given lognormal-distribution model and the open circles are the results reproduced by TBT method. (b) Compares the corresponding SAXS intensities between the given model system and the reproduced one with TBT method.

particle to low-q end. Moreover, the TBT method is always starting from the high-q or small-particle-size end. Consequentially, the errors caused by the previous tangents will add up to the later tangents. Therefore, larger particle size has larger error than smaller particle size. Even so, the largest deviation of particle size is not larger than 10%.

The TBT data analysis method was checked again for a given continuous model system. This model system has a lognormal distribution $P(R)/R$ of particle sizes, in which $P(R)$ is given by equation (7) with the following parameters: $R_0 = 10.0$, $A = 1.0$, $\omega = 0.3$ and $P_0 = 0.0$ as shown in Figure 4a. On the basis of this model system, the SAXS intensity was calculated as shown in Figure 4b. From the calculated SAXS intensity, a PSD function was reproduced by using the TBT method and compared in Figure 4a. The corresponding SAXS intensity was also recalculated and compared in Figure 4b. It can be seen from Figure 4a that the PSD functions have almost the same position and width except a slight difference in profile. This profile difference can be described with a deviation factor as follows:

$$Q = \sqrt{\frac{\sum_i [P_i(actual) - P_i(TBT)]^2}{\sum_i P_i^2(actual)}} \times 100\%, \qquad (9)$$

here, P_i is the occupancy of the ith particle size. The deviation of the above PSD function is about 12%. Figure 4b illustrates also that the recalculated SAXS intensity is in good agreement with the given model.

From the above discussion, we believe that the TBT method can be well used to extract the particle sizes and the corresponding PSD function from SAXS intensity. In order to further validate the dependability of this TBT method, an effective approach to analyze the nanoparticle size distribution [27–29] is used for crosscheck, which is the Polydispersity index (PDI) method. These two methods (i.e., TBT and PDI) are all used to extract the particle size distribution from the in situ SAXS data of PVP-coated Pt nanoparticles at 500 °C. Figure 5 compares the PSD functions and the SAXS fitting curves obtained, respectively, from TBT and PDI methods. Although the profiles of PSD are not exactly the same, the position and width of the two PSD functions are almost the same. Especially, the SAXS fitting curves are all excellently in agreement with the experimental one. Evidently, TBT and PDI methods can give the similar average results for nanoparticle sizes.

Hereafter, the in situ SAXS data of PVP-coated Pt nanoparticles with different temperatures are analyzed by TBT method. The resulting PSD functions at different temperatures are shown in Figure 6a. Obviously, the particle size increases with the temperature increasing, and

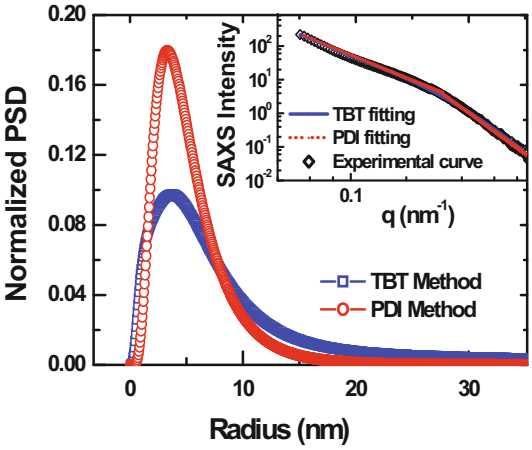

Fig. 5. Comparison of particle size distribution and SAXS intensity between TBT and PDI methods for PVP-coated Pt nanoparticles at 500 °C.

the width of PSD become wider as the temperature is higher than 200 °C. Figure 6b illustrates that the SAXS intensity decays faster with scattering vector, q, when the particle size increases. Except the as-prepared sample at 25 °C, the calculated SAXS intensities are consistent with the experimental ones. The larger derivation at lower-q between the calculated intensity and the experimental one for sample at 25 °C is because of the existence of PVP coating, and its effect on SAXS intensity is not well removed. With increasing temperature, the PVP coating was burnt off and its effect on SAXS intensity is negligible. More important reason of the large deviation for sample at 25 °C is the larger separation of the discrete particle sizes. In this case, the serialization of the discrete particle sizes will cause larger deviation between the calculated SAXS intensity and the experimental one. Figure 6c compares the experimental SAXS intensity and those recalculated, respectively, from the continual PSD and the discrete PSD. It can be seen that the discrete particle sizes obtained from the TBT method can be well used to recalculate the SAXS intensity. As far as we know, heating will cause the growth of nanoparticles. There have been several growth modes for nanoparticles with increasing temperature [6–10]. What has happened to these Pt nanoparticles during heating process?

In order to clarify the growth mode of Pt nanoparticles, TEM observation and in situ XRD experiments during heating were performed. Figure 7 shows the micrograph of TEM for the as-prepared sample at room temperature, its average particle size has been estimated to be about 4 nm. In situ XRD spectra with different sample temperatures are also shown in Figure 8. Two sets of diffraction peaks can be obviously observed. One is from the crystalline lithium fluoride (LiF) which was used as the support materials. Another is from the Pt nanoparticles. The two sets of independent diffraction peaks demonstrate that the Pt nanoparticles have not reacted with the support materials LiF. However, the diffraction peaks from Pt crystallites become sharper with temperature increase, which tell us that the Pt crystallite size increases with the temperature increasing. The crystallite sizes of Pt can be evaluated from the width of the diffraction peaks by using Scherrer's equation. In fact, the width of the diffraction peak is not only caused by the fine crystallite size, but also have the contribution of the instrumental resolution. Fortunately, the influence of the instrumental resolution can be evaluated from the corresponding diffraction peaks of the supporting material LiF. From Figure 8, it can be seen that the widths of the diffraction peaks of LiF are quite narrow compared with those of Pt nanoparticles and almost do not change with temperature increases, which is because the contribution of strain relief and thermal disorder increasing to the width of diffraction peak are almost the same level with temperature change for the LiF crystalline grains. Evidently, the instrumental resolution ($\Delta 2\theta_0$) is not worse than the width (~0.15°) of peak (111) of LiF, i.e., $\Delta 2\theta_0 < 0.15°$. Here, we take the instrumental resolution ($\Delta 2\theta_0$) to be 0.12°, which is corresponding to three pixel-sizes of the image plate detector. The experimental width ($\Delta 2\theta_E$) of Pt (111) reflection is always larger than 0.31° even at 500 °C. Approximately, the diffraction peaks are the convolution of instrument broadening function and the particle-size broadening function. Therefore, the instrumental broadening for the diffraction peaks can be removed by using formula as $\Delta 2\theta_T = ((\Delta 2\theta_E)^2 - (\Delta 2\theta_0)^2)^{1/2}$. The width $\beta (= \Delta 2\theta_T$ in radian) caused by the smaller particle size can be used to estimate the particle size according to the Scherrer's formula $D = K\lambda/(\beta \cos\theta)$. Here, $K = 0.89$, $\lambda = 1.54$ Å, θ is the diffraction angle of Pt (111). The influence of instrumental resolution on the particle sizes is quite small. Especially for the smaller particles ($T < 300$ °C), the broadening of instrumental resolution to the diffraction peaks of Pt nanoparticles is negligible. The crystallite sizes of Pt nanoparticles and the error bars have been evaluated from the width of diffraction peaks of Pt nanoparticles with Scherrer's equation as shown in Figure 9. The average particle sizes of Pt nanoparticles obtained from SAXS data analysis and the error bars are also shown in Figure 9. By comparing Figure 9, we can find that the crystallite sizes obtained from XRD are evidently different from the particle sizes obtained from SAXS, especially for samples at 200 °C and 300 °C. This difference shows us the different structural sensitivity between SAXS and XRD techniques. SAXS is sensitive to the size of fluctuation region of electronic density, but XRD is sensitive to the size of the long-range order region. Therefore, SAXS gives the particle size and XRD presents the crystallite size. The more important is that the difference between SAXS and XRD results reflects the growth mode of nanoparticles during heating process.

By comparing the sizes obtained from SAXS and XRD measurements, it can be found that the starting particle size and crystallite size are nearly the same at room temperature, which has been confirmed by TEM observation as shown in Figure 7. However, the particle sizes obtained from SAXS are, respectively, 6 nm and 28 nm for Pt nanoparticles at 200 °C and 300 °C, but they are

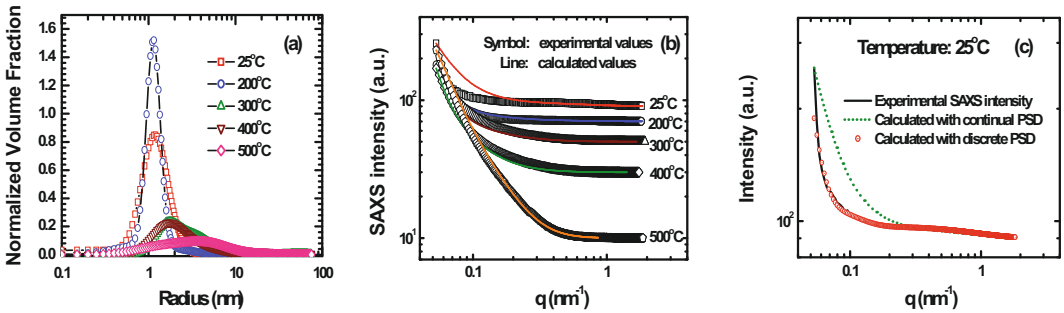

Fig. 6. Particle size distribution (a) and the in situ SAXS intensity comparison (b) of the PVP-coating Pt nanoparticles during heating. (a) Shows that the average particle size increases with temperatures. In (b), the symbols represent the experimental SAXS intensities, the solid lines are the calculated ones based on the PSD in (a). (c) Compares the calculated SAXS intensities by using the discrete and the continual PSDs for sample at 25 °C.

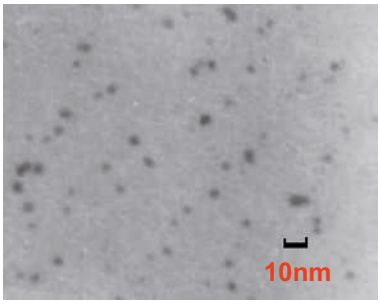

Fig. 7. TEM micrograph of the as-prepared PVP-coated Pt nano-particles at 25 °C. The average particle size is roughly 3–5 nm.

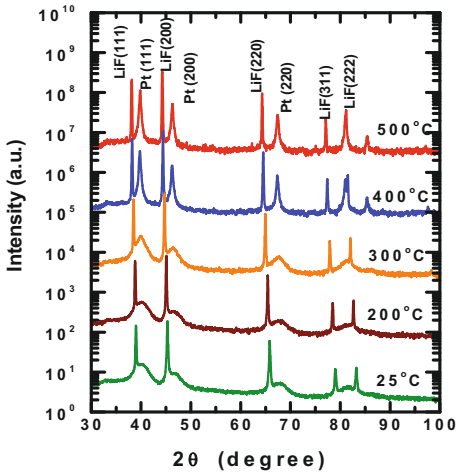

Fig. 8. In situ XRD pattern of PVP-coated Pt nanoparticles during heating. Two sets of diffraction peaks can be, respectively, attributed to the supporting material LiF and the Pt crystallites as indexed in this figure.

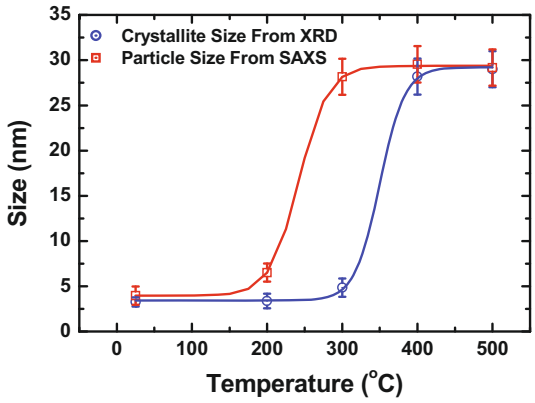

Fig. 9. In situ size change with temperature of the PVP-coated Pt nanoparticles. The open circles are the crystallite sizes deduced from XRD using Scherrer equation; the open squares are the particle sizes calculated from SAXS with TBT method. The solid lines are the guided lines showing a step-like characteristic in both growth of nanocrystallites and nanoparticles.

only 3 nm and 5 nm obtained from XRD. The particles size is about two times larger than the crystallites size at 200 °C, or about six times larger at 300 °C. This implies that crystallite aggregation is the main growth mode of PVP-coated Pt nanoparticles at the heating process. At 400 °C and 500 °C, SAXS gave an average particle-size of 29 nm. These values are almost the same with the crystallite sizes (28 nm at 400 °C and 29 nm at 500 °C) obtained from XRD. The slight difference is possibly because there is an amorphous layer [30] coated on the surface of the nanoparticle or crystallite. However, even considering the error of 10% in particle sizes as discussed above, one particle still contains only one crystallite.

The aggregation process of Pt crystallites to one particle can be described as follows. For the as-prepared Pt nanoparticles at initial state at 25 °C, one particle contains one crystallite. With increasing temperature, there are about two crystallites with different orientations aggregating into one particle at 200 °C. With the temperature increasing up to 300 °C, there are about six Pt crystallites aggregating into one particle in which the crystallites have different orientations. Evidently, there is not enough drive force to make the crystalline aggregates having the same orientation below 300 °C. When the sample temperature is higher than 300 °C, although the size increases still with temperature, averagely, one particle consists of one crystallite. That is to say, multiple crystallites,

which were contained in one particle at lower temperature, have been driven to take the same orientation at higher temperature. This conduces that the Pt crystallites within a nanoparticle have matched the crystal lattice with each other and behave as one crystallite.

The growth tendency of Pt nanoparticles appears a step-like characteristic as shown in Figure 9. Similar characteristic was also presented by high-temperature TEM observation [5]. The largest growth rate are, respectively, 350 °C and 250 °C for crystallites and nanoparticles, which can be estimated by taking the maximum of the first order derivative of size vs. temperature, respectively, from XRD and SAXS results. The largest aggregation degree of multiple crystallites to one nanoparticle occurs at 300 °C. These are consistent with the thermal decomposition temperature of PVP [31].

At the initial temperature, the particle growth is quite slow. With temperature increasing, the particle growth is accelerated. At higher temperature, the particle growth is almost stopped. This change of particle size with temperature is tightly connected with the growth mechanism. Generally speaking, there are several growth modes coexisting in the heating process. Oswald ripening, aggregation and agglomeration are the main manners. According to our SAXS and XRD results, the growth of Pt nanoparticles can be divided into three stages. At the initial stage of heating, PVP is coated on the surface of Pt nanoparticles to form a barrier of nanoparticle growth. Oswald ripening is the main manner of nanoparticle growth. The atoms are transported from the particles smaller than the critical size to the particles larger than the critical size, which makes the smaller particles disappear and the larger ones grow up. The critical size is dependent on the temperature, surface energy and volume energy of a particle. The smaller particles under critical size are not stable. Therefore, this Oswald ripening is quite slow. When the temperature increases further, the nanoparticle growth goes into the second stage. PVP is gradually burnt off, and aggregation becomes the principal growth manner. In this moment, the temperature is high enough to drive the crystallites aggregating together, which accelerates the growth of nanoparticles. At the same time, the number of nanoparticles decreases and the spacing between nanoparticles increases. At higher temperature, evaporation [32] and agglomeration become the main growth manner, and nanoparticle growth goes into the third stage. Because of the long distance between particles and the steric hindrance from the support materials, the nanoparticles' aggregation is difficult. Although the high temperature promotes the atomic evaporation and agglomeration, the larger spacing between particles makes the growth of particle slow or almost stopped.

The particle size obtained from SAXS is a little larger than that obtained from TEM for Pt nanoparticles at room temperature. The reason is that the Pt nanoparticles are coated by PVP at temperature below 200 °C, the scattering intensity came from PVP coating can not be reasonably removed. As the temperature is higher than 200 °C, the PVP coating layers around Pt nanoparticles are partially broken or completely burned off, which makes the Pt nanoparticles naked to each other. This is consistent with the aggregative temperature of Pt nanoparticles starting at 200 °C.

5 Conclusion

In this paper, the TBT method of SAXS data analysis has been discussed and improved, which can be used to deduce the sample's PSD. In situ SAXS and XRD techniques have been used to probe the size change of PVP-coated Pt nanoparticles with temperature. The conclusion can be summarized as follows:

1) The improved TBT method of SAXS data analysis can be effectively used to extract the discrete or continuous PSD from SAXS intensity. The error of this method is about 10%.
2) PVP-coated Pt nanoparticles have been well prepared. In situ SAXS and XRD experiments during heating identify that these nanoparticles' growth experience three stages, i.e., the initial Oswald ripening stage, the middle aggregation growth stage, and the final evaporation and agglomeration growth stage.
3) Combining in situ SAXS and XRD experiments during heating, the growth modes of nanoparticles can be effectively judged according to the change of particle size and crystallite size with temperature. During heating, aggregation is the main growth mode of the PVP-coated Pt nanoparticles.
4) The size change of nanoparticles and nanocrystallites with temperature presents a step-like characteristic. The largest growth rates for Pt nanoparticles and crystallites are, respectively, 250 °C and 350 °C. Moreover, the largest aggregation degree for PVP-coated Pt crystallites occurs at 300 °C.

This work is supported by National Natural Scientific Foundation (No. 10374087) of China and the Knowledge Innovation Program (kjcx3.syw.n8) of Chinese Academy of Sciences.

References

1. P. Kluth, B. Johannessen, D.J. Cookson, G.J. Foran, M.C. Ridgway, Nucl. Inst. Meth. in Phys. Res. B **246**, 30 (2006)
2. I. Lisiecki, H. Sack-Kongehl, K. Weiss, J. Urban, M.P. Pileni, Langmuir **16**, 8802 (2000)
3. D.V. Talapin, A.L. Rogach, M. Haase, H. Weller, J. Phys. Chem. B **105**, 12278 (2001)
4. G. Sandi, R.E. Winans, S. Seifert, K.A. Carrado, Chem. Mater. **14**, 739 (2002)
5. Mikihisa Mizuno, Yuichi Sasaki, A.C.C. Yu, Makoto Inoue, Langmuir **20**, 11305 (2004)
6. G.P. Glaspell, P.W. Jagodzinski, A. Manivannan, J. Phys. Chem. B **108**, 9604 (2004)
7. Shaofeng Ran, C. Burger, Dufei Fang, Xinhua Zong, Benjamin Chu, Benjamin S. Hsiao, Yasuo Ohta, Kazuyuki Yabuki, P.M. Cunniff, Macromolecules **35**, **27**, 9851 (2002)

8. A. Guinier, G. Fournet, *Small-Angle Scattering of X-rays* (Wiley, New York, 1955)
9. H.K. Kammler, G. Beaucage, D. Kohls, N. Agashe, J. Ilavsky, J. Appl. Phys. **97**, 054309 (2005)
10. M. Sztucki, T. Narayanan, G. Beaucage, J. Appl. Phys. **101**, 114304 (2007)
11. H.K. Kammler, G. Beaucage, R. Mueller, S.E. Pratsinis, Langmuir **20**, 1975 (2004)
12. T. Teranishi, M. Hosoe, T. Tanaka, M. Miyake, J. Phys. Chem. B **103**, 3818 (1999)
13. Zhongjun Chen, Zhonghua Wu, Minhua Sun, Xing Chen, Quan Cai, Shishun Yang, High Energy Physics and Nuclear Physics **29**, 321 (2005)
14. http://www.esrf.eu/computing/scientific/FIT2D
15. Wei Wang, Xing Chen, Quan Cai, Guang Mo, Zhongjun Chen, Zhihong Li, Kunhao Zhang, Zhonghua Wu, Nuclear Techniques **30**, **7**, 571 (2007)
16. A.V. Semenyuk, D.I. Svergun, J. Appl. Cryst. **24**, 537 (1991)
17. http://www.insp.jussieu.fr/axe2/Oxydes/IsGISAXS/isgisaxs.htm
18. L.C. Roess, C.G. Shull, J. Appl. Phys. **18**, 308 (1947)
19. L.C. Roess, C.G. Shull, J. Appl. Phys. **18**, 295 (1947)
20. M.H. Jellinek, H. Solomon, I. Fankuchen, Ind. Eng. Chem. **18**, **3**, 172 (1946)
21. D.I. Svergun, J. Appl. Cryst. **24**, 485 (1991)
22. C.G. Vonk, J. Appl. Cryst. **9**, 433 (1976)
23. O. Glatter, J. Appl. Cryst. **10**, 415 (1977)
24. J. Riseman, Acta. Cryst. **5**, 193 (1952)
25. M.H. Jellinek, I. Fankuchen, Ind. Eng. Chem. **41**, **10**, 2259 (1949)
26. G. Herdan, Small Particle Statistics, London Chap. 6 (1960)
27. G. Beaucage, H.K. Kammler, S.E. Pratsinis, J. Appl. Cryst. **37**, 523 (2004)
28. G. Beaucage, J. Appl. Cryst. **28**, 717 (1995)
29. G. Beaucage, J. Appl. Cryst. **29**, 134 (1996)
30. Hsin Lung Chen, Ming Siao Hsiao, *Macromolecules* **31**, 6579 (1998)
31. Y. Borodko, S.E. Habas, M. Koebel, Peidong Yang, H. Frei, G.A. Somorjai, J. Phys. Chem. B **110**, 23052 (2006)
32. K.K. Nanda, F.E. Kruis, H. Fissan, Phys. Rev. Lett. **89**, 256103 (2002)